ELSEVIER

Physics of the Earth and Planetary Interiors 127 (2001) 51–66

PHYSICS OF THE EARTH AND PLANETARY INTERIORS

www.elsevier.com/locate/pepi

Implications of slab mineralogy for subduction dynamics

Craig R. Bina*, Seth Stein, Frederic C. Marton[1], Emily M. Van Ark

Department of Geological Sciences, Northwestern University, Evanston, IL, USA

Received 30 March 2000; accepted 14 December 2000

Abstract

Phase relations among mantle minerals are perturbed by the thermal environment of subducting slabs, both under equilibrium and disequilibrium (metastable) conditions. Such perturbations yield anomalies not only in seismic velocities but also in density. The buoyancy forces arising from these density anomalies may exert several important effects. They contribute to the stress field within the slab, in a fashion consistent with observed patterns of seismicity. They may affect subduction rates, both by inducing time-dependent velocity changes under equilibrium conditions and by imposing velocity limits through a thermal feedback loop under disequilibrium conditions. They may affect slab morphology, possibly inhibiting penetration of slabs into the lower mantle and allowing temporary stagnation of deflected or detached slabs. Latent heat release from phase transitions under disequilibrium conditions in slabs can yield isobaric superheating, which may generate adiabatic shear instabilities capable of triggering deep seismicity. © 2001 Elsevier Science B.V. All rights reserved.

Keywords: Slab mineralogy; Subduction; Morphology

1. Introduction

Subducting slabs sink into the mantle because they are negatively buoyant. Much of this negative buoyancy is thermal, arising from the temperature difference between cold slab and warm mantle material. Thus colder slabs, such as those of greater age and/or faster subduction rates, should possess greater negative thermal buoyancies (McKenzie, 1969; Elsasser, 1969; Minear and Toksöz, 1970; Forsyth and Uyeda, 1975; Becker et al., 1999). There are, however, additional important sources of slab buoyancy. Temperature contrasts between subducting slab and ambient mantle imply that the equilibrium depths of chemical reactions, such as subsolidus phase transformations between low- and high-pressure mineral phases, will differ between slab and mantle, and the consequent lateral juxtaposition of phase assemblages of differing densities must generate additional "petrological" buoyancy forces. Furthermore, the low temperatures within slabs also may give rise to disequilibrium effects due to kinetic hindrance of reactions, such as metastable persistence of low-pressure minerals into the stability fields of high-pressure phases, and the resulting spatial variations in mineralogy will also contribute to petrological buoyancy forces.

These buoyancy forces, both thermal and petrological, have important effects on the physical behavior of subducting slabs. The spatial distribution of buoyancy forces contributes to the stress field within slabs, and these stresses may be reflected in patterns of seismicity. Additionally, spatial and temporal variations in the net buoyancies of slabs may be reflected in varying subduction rates, through changes in the important "slab pull" driving forces for surface plate

* Corresponding author. Fax: +1-847-491-8060.
E-mail address: craig@earth.northwestern.edu (C.R. Bina).
[1] Present address: Geophysical Laboratory, Carnegie Institution of Washington, Washington, DC, USA.

0031-9201/01/$ – see front matter © 2001 Elsevier Science B.V. All rights reserved.
PII: S0031-9201(01)00221-7

motions. Furthermore, these buoyancy forces may affect slab morphology, such as the lateral deflection of some slabs at the top of the lower mantle. Finally, the thermal perturbation of phase relations which gives rise to the petrological buoyancy forces may also influence the thermal evolution of slab material, through latent heats of reaction.

2. Phase relations

To study these effects, we begin by constructing a simple thermal model of a subduction zone. For the example shown in Fig. 1, a two-dimensional numerical model of the temperature distribution within a subduction zone was calculated on a 120 × 90 grid for lithosphere of 140-Ma age subducting at 8 cm per year at a dip angle of 60°, using a simple finite difference algorithm (Minear and Toksöz, 1970; Toksoz et al., 1973) that neglects both shear and radiogenic heating, with initial lithospheric temperatures derived from the plate model GDH1 (Stein and Stein, 1992). To construct a mineralogical model that corresponds to this thermal structure, we first supplement this thermal structure with simple representations of pressure and composition. Here, the variation of pressure with depth is obtained by radial integration of the reference density model PEMC (Dziewonski et al., 1975). For simplicity, the bulk chemical composition is assumed to be uniformly that of $(Mg_{0.9}Fe_{0.1})_2SiO_4$ mantle olivine (Ringwood, 1982), although more sophisticated models might take into account compositional layering within slabs (Helffrich et al., 1989). From such a map of temperature, pressure, and bulk composition at each point of interest, we can determine the stable mineral assemblages at each corresponding point. Mineral phase assemblages are determined by free energy minimization, using a simulated annealing algorithm (Bina, 1998a) and thermodynamic parameters (Fei et al., 1991) for olivine (α), its polymorphs wadsleyite (β) and ringwoodite (γ), and its disproportionation products magnesiowüstite (mw) and ferromagnesian silicate perovskite (pv).

Two resulting models are shown in Fig. 2: the equilibrium case, and a disequilibrium case in which α olivine persists metastably at temperatures below 1000 K (Sung and Burns, 1976a,b; Green and Burnley, 1989; Kirby et al., 1991; Rubie and Ross, 1994; Green and Houston, 1995; Kirby et al., 1996; Kerschhofer et al., 1996; Wang et al., 1997). While this latter representation of the limits of metastability as a simple isothermal cutoff is an oversimplification of the complex kinetics of the olivine transformations (Liu et al., 1998), it is sufficient to illustrate the first-order buoyancy effects. As expected, perturbation of equilibrium phase relations in the mantle (Turcotte and Schubert, 1971, 1972; Schubert et al., 1970, 1975; Bina, 1996) by the cold slab results in upward deflection (due to their positive Clapeyron slopes) of the $\alpha \rightarrow \alpha+\beta \rightarrow \beta$ and the $\beta \rightarrow \beta+\gamma \rightarrow \gamma$ transitions from their nominal depths of ~410 and ~530 km, respectively, as well as downward deflection (due to its negative Clapeyron slope) of the $\gamma \rightarrow \gamma + \text{pv} + \text{mw} \rightarrow \text{pv} + \text{mw}$ transition from its nominal depth of ~660 km (Navrotsky, 1980; Akaogi et al., 1989; Katsura and Ito, 1989; Ito and Takahashi,

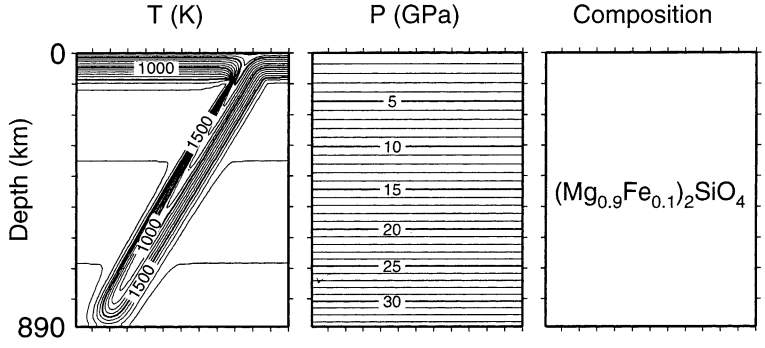

Fig. 1. Sample pressure, temperature, and compositional model for a simple model of a subducting slab (140-Ma lithosphere subducting at 8 cm per year at 60° dip) (modified from Bina (1998a)).

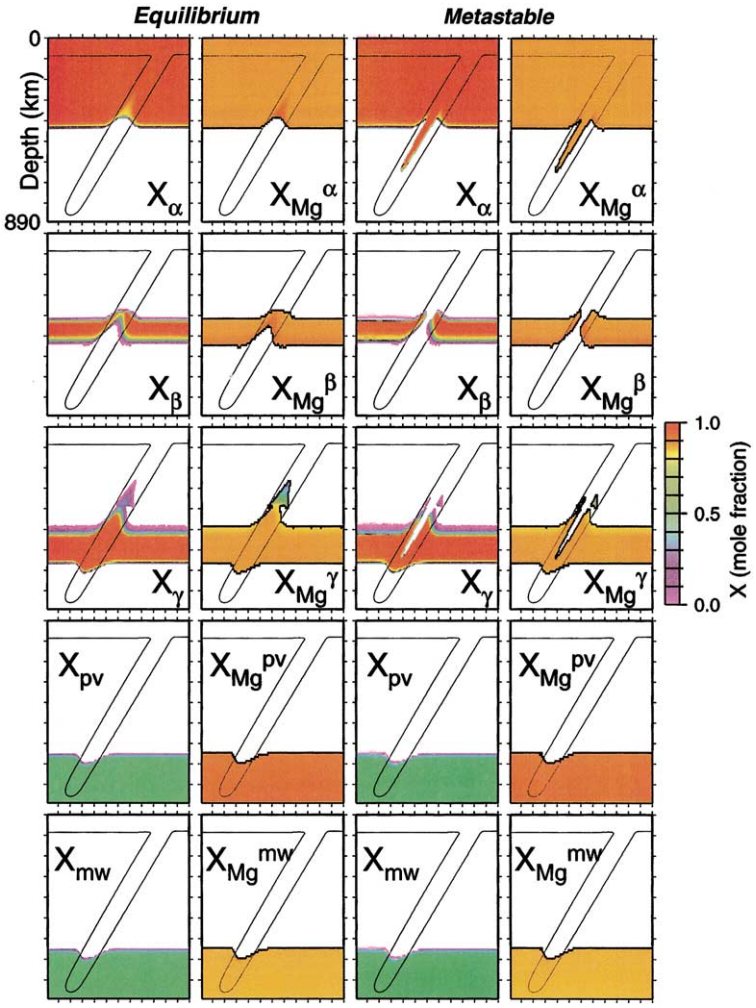

Fig. 2. Molar phase distribution (X_ϕ) and composition (X_{Mg}^{ϕ}) for equilibrium and disequilibrium (metastable) cases. Also shown is 1500 K isotherm (modified from Bina (1996, 1998a)).

1989; Ito et al., 1990; Akaogi and Ito, 1993; Bina and Helffrich, 1994; Green and Houston, 1995; Bina, 1996, 1997; Helffrich, 2000). However, solid-solution effects in the $(Mg_{0.9}Fe_{0.1})_2SiO_4$ bulk composition dictate that these are not simple deflections of univariant phase boundaries. In these divariant reactions, the relative proportions of the phases change continuously over narrow depth intervals, rather than discontinuously as would occur in a pure Mg_2SiO_4 composition. Furthermore, within the coldest core of the slab, the usual $\alpha \rightarrow \alpha + \beta \rightarrow \beta \rightarrow \beta + \gamma \rightarrow \gamma$ sequence of upper mantle transitions is replaced by the $\alpha \rightarrow \alpha + \gamma \rightarrow \beta + \gamma \rightarrow \gamma$ series (Green and Houston, 1995), in which Fe-rich γ becomes stable along with Fe-poor α at relatively shallow depths (Bina, 1996), prior to subsequent transformation of this $\alpha + \gamma$ to a $\beta + \gamma$ assemblage. These effects also can be seen in Fig. 3, which shows the nonlinear variation (Helffrich and Bina, 1994; Stixrude, 1997) of phase proportions and compositions along down-dip profiles through the temperature minimum of the slab as well as a vertical profile through the surrounding mantle. The results for the disequilibrium case are broadly similar to those for the equilibrium

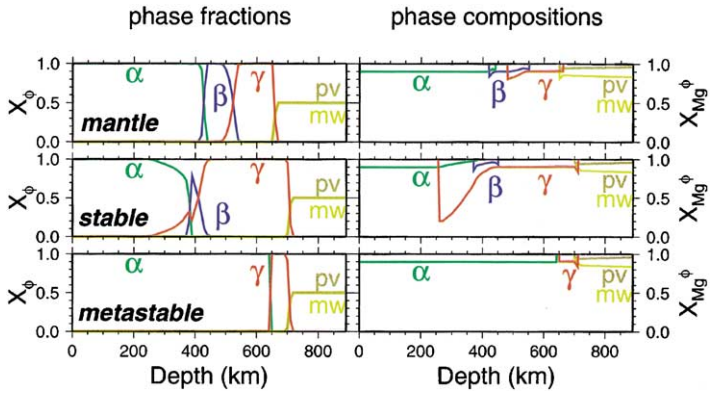

Fig. 3. Profiles of molar phase distribution (X_ϕ) and composition (X^ϕ_{Mg}) vs. depth, for ambient mantle and along slab temperature minimum for equilibrium (stable) and disequilibrium (metastable) cases (modified from Bina (1996)).

case, except that in the former a tongue of α extends metastably to great depths within the coldest core of the slab (Fig. 3). The portions of Figs. 2 and 3 which depict the phase proportions for these two cases are coarsely summarized in the upper panels of Fig. 4.

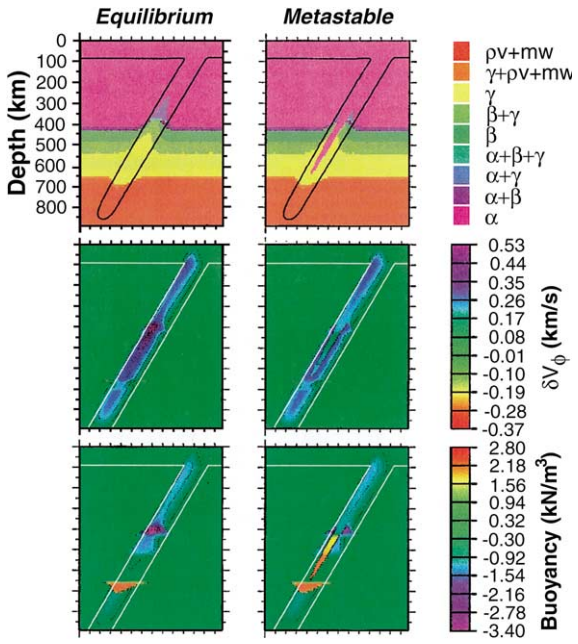

Fig. 4. Phase assemblages (top), bulk sound velocity anomalies (middle), and buoyancy anomalies (bottom) for equilibrium and disequilibrium (metastable) cases. Also shown is 1500 K isotherm (top) and slab boundary (middle and bottom). $V_\phi^2 = V_P^2 - (4/3)V_S^2$ (modified from Bina (1997, 1998a)).

Given our choice of a bulk composition of pure olivine stoichiometry, this simple analysis treats only reactions within $(Mg, Fe)_2SiO_4$ olivine, which forms perhaps 55–65% by volume of a peridotite mantle. The remaining $(Ca, Mg, Fe)SiO_3 \cdot Al_2O_3$ pyroxene (px) and garnet (gt) phases also undergo phase transformations, to silicate ilmenite (il), majoritic garnet (mjgt), and both calcic and ferromagnesian silicate perovskites (pv). However, such transitions as px + gt → px + mjgt → mjgt and mjgt → mjgt + pv → pv should be broader in depth-extent by about an order of magnitude than the transitions in olivine (Bina and Wood, 1984; Akaogi et al., 1987; Bina and Liu, 1995; Wood and Rubie, 1996; Vacher et al., 1998), and their contributions to local density anomalies and hence buoyancy forces should be considerably more diffuse. Indeed, the breadth of transitions involving garnet-bearing assemblages reflects their highly multivariant nature, so that in a natural multicomponent system they may not possess meaningful Clapeyron slopes (which are strictly defined only for univariant reactions).

3. Buoyancy anomalies

The lateral juxtaposition of high- and low-pressure phase assemblages resulting from this perturbation of mantle phase relations by the slab's thermal field implies anomalies in both seismic velocity and density relative to the surrounding mantle (Richter, 1973;

Schubert et al., 1975; Christensen and Yuen, 1984, 1985; Ito and Sato, 1992; Bina, 1996, 1997, 1998a; Yoshioka et al., 1997; Koper and Wiens, 2000), and the action of gravity upon these density anomalies gives rise to buoyancy anomalies (Fig. 4) which are superimposed on the negative thermal buoyancy of the slab (also reflected in overall fast seismic velocities). The upward equilibrium deflection of the $\alpha \rightarrow \beta \rightarrow \gamma$ phase transitions yields negative buoyancies (also reflected in locally faster velocity anomalies) at shallow depths, by stabilizing dense high-pressure phases in the cold slab that are surrounded by less dense lower-pressure phases in the ambient mantle. Furthermore, the downward equilibrium deflection of the $\gamma \rightarrow \mathrm{pv} + \mathrm{mw}$ transition yields positive buoyancies (also reflected in locally slower velocity anomalies) at greater depths, by allowing less dense phases in the cold slab to persist stably to depths where they are surrounded by denser higher-pressure phases in the mantle. On the other hand, in the disequilibrium case where α persists metastably beyond its stability field, the resulting tongue of metastable α implies positive buoyancy anomalies at depth, which should also be reflected in locally slow velocity anomalies.

It is worth noting that despite the attractive features of the disequilibrium metastability model, seismological studies have failed to clearly detect direct evidence of a metastable wedge (Iidaka and Obara, 1997; Helffrich, 1998; Koper et al., 1998; Collier and Helffrich, 1997, 2000). Although the low seismic-velocity wedge (Fig. 5) within the complex geometry of the high-velocity slab is likely to be an elusive target (years of study having been required to observe trapped seismic waves for the analogous case of low-velocity fault interiors), whose detection will be further complicated by additional non-olivine components (Hogrefe et al., 1994; Vacher et al., 1999), current seismological results are most easily explained by the absence of such a coherent wedge. On the other hand, recent failures to detect fast seismic velocity anomalies in a slab (using earthquakes outboard of a subduction zone) do suggest chemical or petrological counterweights to low slab temperatures (Brudzinski et al., 1997; Brudzinski and Chen, 2000), such as partial melt or volumes (either coherent or distributed) of metastable olivine.

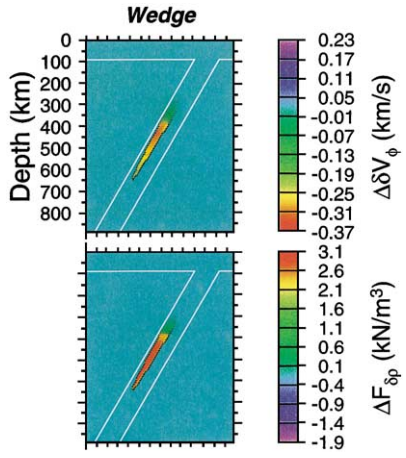

Fig. 5. Differential bulk sound velocity anomalies (top) and buoyancy anomalies (bottom) between disequilibrium and equilibrium cases, showing predicted effect of metastable olivine wedge. Also shown is slab boundary (modified from Bina (1998a)).

4. Stress fields

The spatial distribution of the buoyancy anomalies arising from the thermal perturbation of equilibrium phase relations (Fig. 4) suggests that material between the regions of deflected phase transitions may be compressed by the opposed buoyancy forces (Griggs, 1972; Goto et al., 1987; Ito and Sato, 1992; Bina, 1996, 1997; Yoshioka et al., 1997). We can calculate the principal stresses arising from these buoyancy forces, using a finite-element method (Gobat and Atkinson, 1995) with 4-node isoparametric elements for an elastic medium with spatially varying moduli. For this simplest case, we model both the slab and mantle as purely elastic media, albeit with elastic moduli which vary spatially due to variations in pressure, temperature, and phase assemblage. Solution for the displacements and stresses which minimize the strain energy at static equilibrium (Segerlind, 1984), yields significant down-dip compressional stresses in this region (Fig. 6). It is the opposition of these buoyancy forces through the depth interval of the transition zone, rather than any single buoyancy anomaly alone, which gives rise to this stress pattern in the slab (Bina, 1997).

The down-dip slab stresses change from tensional to compressional near ∼400 km depth, with down-dip compressional stresses persisting to ∼690 km, below which compressional stresses cease. This pattern is

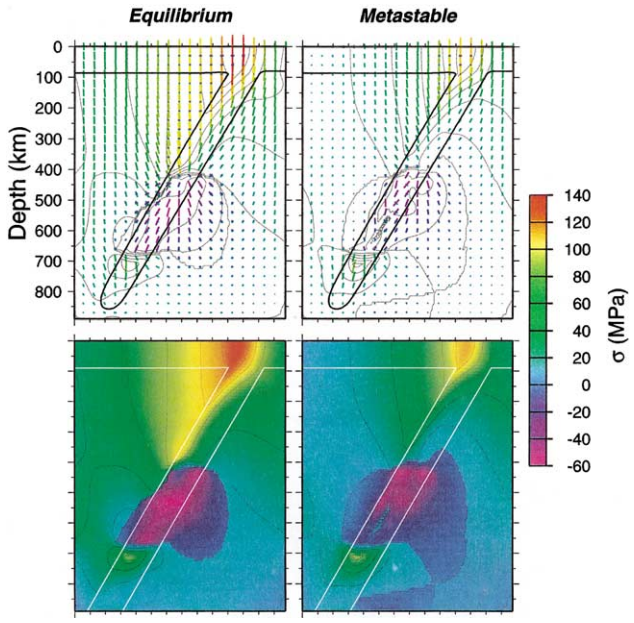

Fig. 6. Principal stresses, shown as vectors (top) and as maximum absolute magnitudes (bottom), calculated for an elastic rheology, for equilibrium and disequilibrium (metastable) cases. Negative stresses are compressional; positive stresses are extensional. Also shown is 1500 K isotherm (top) and slab boundary (bottom) (modified from Bina (1997)).

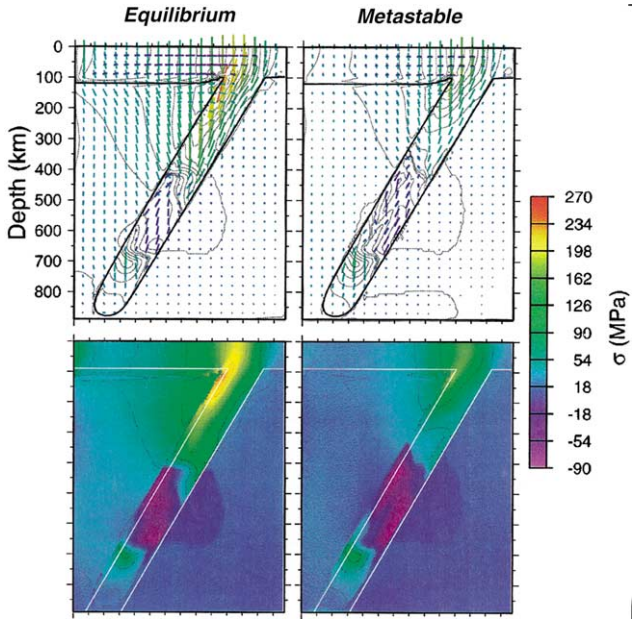

Fig. 8. Principal stresses, shown as vectors (top) and as maximum absolute magnitudes (bottom), calculated for an elastic slab within a Maxwell viscoelastic mantle ($t = 6$ ky), for equilibrium and disequilibrium (metastable) cases. Also shown is 1700 K isotherm (top), which delimits elastic–viscoelastic transition, and slab boundary (bottom).

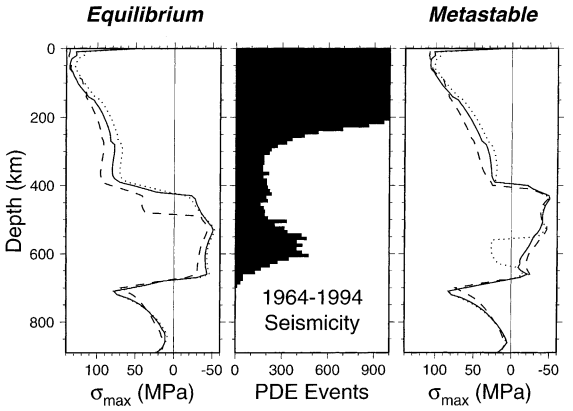

Fig. 7. Magnitude of the absolute maximum principal stress profiled down-dip along slab temperature minimum (solid), for equilibrium and disequilibrium (metastable) cases. Also shown are down-dip profiles along lines 25 km above (dashed) and below (dotted) the temperature minimum, measured normal to the slab. Center panel shows depth distribution of global seismicity for 1964–1994 from PDE catalogue (modified from Bina (1997)).

in good agreement with observed patterns of deep seismicity (Isacks and Molnar, 1971; Vassiliou et al., 1984; Rees and Okal, 1987; Vassiliou and Hager, 1988; Frohlich, 1989; Okal and Bina, 1998), for which down-dip compressional focal mechanisms are generally observed, as can be seen by comparing the depth distribution (NEIC, 1994) of global seismicity with down-dip profiles of maximum principal stress along the temperature minimum of the slab's interior (Fig. 7). Furthermore, the larger compressive stresses are of the same order as the larger stress drops estimated for deep earthquakes (Houston and Williams, 1991). Moreover, the transition from down-dip extensional to compressional stress near 400 depth corresponds roughly to the observed minimum in deep seismicity around 300–400 km depth, and the termination of down-dip compression near 700 km depth is in accord with the observed cessation of seismicity below that depth. The large extensional stresses in the wedge-slab corner and the large compressional stresses in the mantle outside the deep slab are boundary artifacts of our simple model of static stresses in a purely elastic medium, whose relative magnitudes will begin to decline when we introduce a more realistic rheology below.

Calculated stress patterns in this simple elastic model for the disequilibrium case of metastable persistence of α are similar, except that the presence of a positively buoyant tongue of α within the negatively buoyant interior of the slab results in a narrow interior region in which the absolute maximum principal stress is tensional and not oriented down-dip (Fig. 6). This effect, together with slightly rotated stresses of decreased compressional magnitude in the outer portions of the slab, shifts the compressive stress maximum toward somewhat shallower depths (Fig. 7).

In these simple stress models for purely elastic media, the region of large compressive stresses extends beyond the boundaries of the slab and into the mantle. However, the rheology of the cold slab may differ significantly from that of the warmer mantle, and a viscous mantle is unlikely to respond purely elastically (Karato, 1997). This issue may be addressed by incorporating a more complex rheology, such as viscoelasticity, into the finite-element model (Northwest, 1998). For example, we may take the same purely elastic slab but embed it in a viscoelastic mantle, retaining the same spatially varying elastic moduli. Here, the mantle exhibits Maxwell viscoelasticity in which the shear moduli relax with a viscosity of 10^{21} Pa s, and the cutoff between elastic and viscoelastic behavior is modeled as the 1700 K isotherm. In this case (Fig. 8), the down-dip compressive stresses become concentrated within the slab itself (Bina and Kirby, 1999). Furthermore, in the disequilibrium case the zone of maximum compressive stress divides into two regions lying above and below the metastable wedge. Some anomalous shallow wedge stresses and bleeding of compressional stresses into the mantle below the slab remain, as boundary artifacts of our simple static model, but they continue to decline with greater relaxation times (Ken Kumayama, personal communication). A more thorough analysis might incorporate a fully viscoelastic model in which both mantle and slab viscosities vary with both temperature and pressure, but ultimately a fully dynamical model involving mantle return flow would be necessary to resolve fine structure. Moreover, use of a variety of regionally appropriate thermal models would allow comparison of consequent stress patterns with seismicity profiles for various individual subduction zones (Helffrich and Brodholt, 1991), rather than simply with a global ensemble.

Other studies (Goto et al., 1987; Devaux et al., 1999) have suggested that transformational strain

associated with heterogeneous volume changes along the boundaries of a metastable wedge would generate stresses much larger than those associated with thermal strain and buoyancy forces. However, these studies have not incorporated the effects of stress relaxation across phase changes (Karato, 1997; Riedel and Karato, 1997), nor have they included the $\gamma \rightarrow$ pv + mw transition whose buoyancy force plays an important role in generating large down-dip compressive stresses in the slab (Bina, 1997).

5. Subduction rates

The spatial distribution of buoyancy anomalies associated with the thermal perturbation of phase relations (Fig. 4) also suggests the potential for temporal variations in subduction rates (Bassett, 1979; Rubie, 1993; Kirby et al., 1996; Marton et al., 1999a; Schmeling et al., 1999). Shortly after initiation of subduction, a slab will be negatively buoyant due simply to negative thermal buoyancy. Some time thereafter, the sinking slab will reach the equilibrium depth of the first of the uplifted phase transitions, gaining additional negative buoyancy due to the petrological contribution, which should increase the slab's rate of descent. Eventually the slab will reach the equilibrium depth of the downwardly deflected transition, where it will acquire a positive petrological buoyancy contribution. Although the slab may remain negatively buoyant in the aggregate, the attendant decrease in the downward buoyancy force should decrease its rate of descent (Marton et al., 1999a; Schmeling et al., 1999).

This effect can be seen in Fig. 9, where the terminal velocity of our model slab (from Fig. 1) as a function of penetration depth is estimated by equating the down-dip component of the slab's aggregate (mean summed) buoyancy force with the total viscous drag force. The latter is determined for the two sides of the slab, given by the product of length and shear stress, and for a semicircular slab tip, given by the half the Stokes's law value (Batchelor, 1967), for a slab of fixed geometry sinking through a mantle of viscosity 3.7×10^{20} Pa s (Mitrovica and Peltier, 1993). The resulting variations in subduction rate are on the order of a few cm per year as the slab penetrates the transition zone (Marton et al., 1999a). While

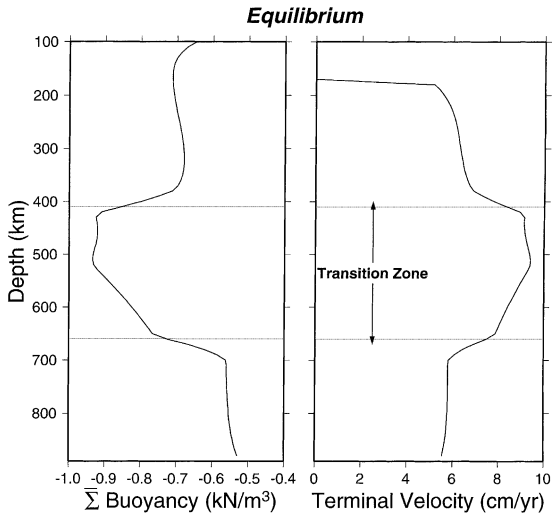

Fig. 9. Variation of slab's mean summed buoyancy force (left) and calculated terminal velocity (right) with slab penetration depth, for equilibrium case (modified from Marton et al. (1999a)).

most proposed mechanisms for changes in surface plate motions involve relatively gradual changes in velocity (Lithgow-Bertelloni and Richards, 1998), such time-dependent changes in bulk slab buoyancy, and hence subduction rate, with depth of penetration may provide a mechanism for more rapid changes. Note, however, that this mechanism generates changes in descent velocities only when a slab first encounters the transition zone, so that subduction occurs at a steady rate after the slab penetrates into the lower mantle.

In the disequilibrium case of metastable persistence of α within slabs, the positive buoyancy of a wedge of metastable α should act to further decrease subduction rates. Moreover, colder slabs, which should sink faster due to their greater negative thermal buoyancy, should have their descent rates slowed more by their larger metastable wedges (Bassett, 1979; Rubie, 1993; Kirby et al., 1996; Schmeling et al., 1999; Marton et al., 1999a). This "parachute effect", in which olivine metastability reduces subduction velocities for colder slabs, can be seen in Fig. 10. Here, we abandon our simple isothermal-cutoff model of metastability in favor of simple rate laws of transformation kinetics which are experimentally constrained (Rubie and Ross, 1994).

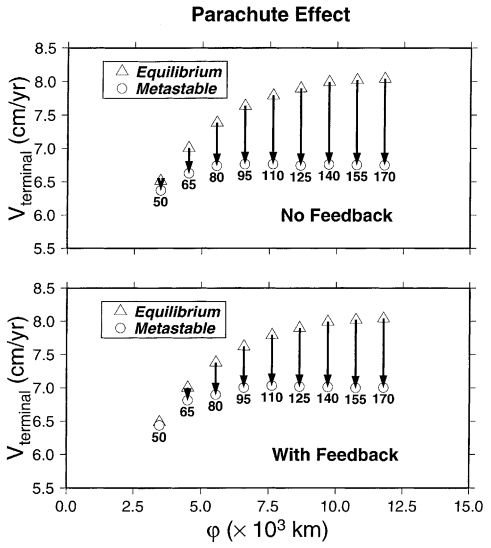

Fig. 10. Calculated terminal velocities, for equilibrium case (triangles) and disequilibrium (metastable) case (circles), showing the parachute effect (arrows) by which larger metastable wedges slow colder slabs to a greater extent. The thermal parameter (ϕ) is controlled by varying the age of lithosphere at the trench (numbers, in Ma). Magnitude of effect predicted by simple calculation (top) is damped by inclusion of feedback phenomenon (bottom) (modified from Marton et al. (1999a,b)).

The thermal state of the slab is represented simply by its "thermal parameter" (ϕ) — given by the product of the trench-normal convergence rate, the sine of the slab dip, and the age of the lithosphere entering the trench — so that larger thermal parameters correspond to colder (older and/or more rapidly subducting) slabs (Molnar et al., 1979; Gorbatov et al., 1996; Marton et al., 1999a). Slab thermal models are calculated using the same simple finite difference method (Minear and Toksöz, 1970). Colder slabs, which would sink faster in the equilibrium case, are slowed more than warmer slabs by their metastable olivine "parachutes" (Marton et al., 1999a; Schmeling et al., 1999). Moreover, such slowing, of the order of one cm per year, enters into a negative feedback loop. While colder slabs have larger metastable wedges and are slowed more due to the parachute effect, this deceleration exposes them to greater conductive warming which thermally erodes their wedges, so the resulting loss of positive buoyancy will accelerate their sinking somewhat. This feedback damps the amplitude of the parachute effect (Fig. 10), but the net effect is still to slow the rates of slab descent (Marton et al., 1999b; Tetzlaff and Schmeling, 2000). Such feedback damping may act to limit (Gordon, 1991) the allowable range of subduction rates (Marton et al., 1999a,b; Tetzlaff and Schmeling, 2000). However, it should be noted that the nature of such speed limits remains a matter of some uncertainty. The model shown here predicts that the velocities of slabs containing metastable olivine should approach a limiting value with increasing age of the slab (Marton et al., 1999a). Other, fully dynamical, models have suggested that these velocities should decrease (Schmeling et al., 1999) or continue to increase (Tetzlaff and Schmeling, 2000) with increasing age of the slab. Resolution of this issue awaits more sophisticated modeling and better understanding of rheological constraints (Tetzlaff and Schmeling, 2000).

6. Slab morphology

For extremely cold slabs, a metastable wedge may be so large as to render the slab positively buoyant in the aggregate for penetration below some critical depth. This can be seen in Fig. 11, in which a thermal model for the very cold Tonga slab (Bevis et al., 1995) yields a wedge of metastable α whose kinetically limiting 1000 K isotherm extends so deeply that the slab is positively buoyant if it penetrates directly into the lower mantle (Bina and Kirby, 1999). Thus, the metastable wedge imposes a "petrological buoyancy cost" negating the negative thermal buoyancy that drives subduction. These buoyancy forces should produce very large slab compressive stresses in the transition zone as well as large bending moments (Lundgren and Giardini, 1992, 1994; Lay, 1994; van der Hilst, 1995; Bina, 1996, 1997; Bina and Kirby, 1999) associated with upward deflection of the slab below 660 km. Equilibrium depression of the $\gamma \rightarrow \mathrm{pv} + \mathrm{mw}$ transition alone contributes a significant positive buoyancy increment to the slab at the base of the upper mantle (Fig. 11), but it is the large magnitude and extent of the positive buoyancy associated with a metastable wedge (the same buoyancy that limits subduction velocities through the parachute effect discussed above) which allows the

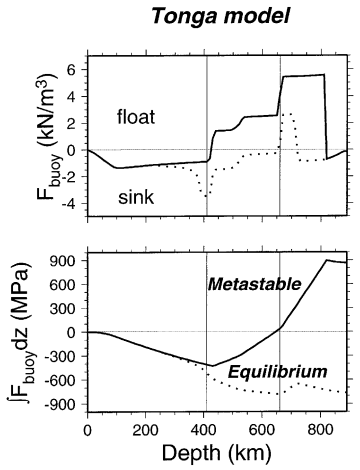

Fig. 11. Buoyancy force (top) and depth-integrated buoyancy force (bottom), profiled down-dip along slab temperature minimum, for a cold Tonga slab model (120 Ma lithosphere at 24 cm per year and 40°), for equilibrium and disequilibrium (metastable) cases. Vertical lines delimit the transition zone. Slab with large metastable wedge becomes positively buoyant upon entering the lower mantle (modified from Bina and Kirby (1999)).

net buoyancy of the slab to become neutral or even positive. The net effect of these buoyancy forces is to deflect the slab toward the horizontal at the base of the transition zone (Tetzlaff and Schmeling, 2000). Stagnation of slab material near the depth of neutral buoyancy should persist until thermal erosion of the positively buoyant metastable wedge by conductive warming allows the slab to resume sinking under the influence of its residual negative thermal buoyancy (Bina and Kirby, 1999; Tetzlaff and Schmeling, 2000).

Such increased resistance to slab descent into the lower mantle beneath Tonga is consistent with tomographic images and the distribution of deep seismicity, which together suggest the presence of recumbent slab material up to 750 km west of the base of the inclined Wadati–Benioff zone (van der Hilst, 1995; Zhao et al., 1997; Okal and Kirby, 1998; Deal and Nolet, 1999; Fukao et al., 2001), as well as with apparent depression of the $\gamma \rightarrow \mathrm{pv} + \mathrm{mw}$ transition to the west of the base of the inclined Wadati–Benioff zone (Roth and Wiens, 1999). It is also consistent with the observed (Po-Fei Chen, personal communication) unusual upward extension of the down-dip compressional stress regime of deep earthquakes to intermediate depths in Tonga. Interestingly, the strongest evidence for subhorizontal deflection of the Tonga slab derives from the northern end of the Tonga arc (Deal and Nolet, 1999). This appears to correspond to the region of highest subduction rates (Bevis et al., 1995) and thus presumably to the region of lowest slab temperatures and greatest potential for mineral metastability. Just as in the case of the parachute effect, a feedback loop may be involved, if slab deflection also acts to slow descent rates thereby raising slab temperatures and limiting the extent of metastability, but dynamical models suggest that the amount of such slowing should be small even for large subhorizontal deflections of the slab (Tetzlaff and Schmeling, 2000).

In addition to the case of deflected slabs, there is that of detached slabs. The deep seismicity beneath the North Fiji Basin, for example, is thought to occur in a slab of former Pacific plate that was subducted at the Vitiaz trench and then detached during a late Miocene arc reversal (Okal and Kirby, 1998). Thermokinetic modeling suggests that a metastable wedge of significant extent is unlikely to survive the thermal evolution of most such pieces of detached slab (Van Ark et al., 1998). In such models, combining slab thermal evolution (Marton et al., 1999a) with olivine transformation kinetics (Rubie and Ross, 1994), a cold wedge of metastable α olivine rapidly achieves a steady-state size. This initial size is characteristic of the thermal parameter of subduction, in that colder slabs develop larger wedges. Upon detachment of the lower reaches of the slab from its overlying portion, modeled as occurring in the uppermost mantle near the depth of the base of the overriding lithosphere, the metastable wedge remains of roughly constant size until the detachment surface enters the transition zone. Thereafter, enhanced thermal erosion effectively inverts the association of large metastable wedges with initially cold slabs. Because colder slabs sink faster, they spend more time surrounded by hotter material (at greater depths), and their metastable wedges thermally erode more rapidly. Thus, colder slabs form larger wedges, but upon slab detachment these large wedges decay faster. For a range of simple thermal models of Vitiaz plate geometry and evolution (Gordon and Jurdy, 1986; Hamburger and Isacks, 1987; Greene et al., 1994), calculated using the same finite difference method

(Minear and Toksöz, 1970) with Tonga-like parameters (100 Ma lithosphere at 14 cm per year and 60°), the large metastable wedge is reduced in size to a few tens of percent of its initial extent by ∼10 My after detachment. Thus, any faulting nucleated within any metastable material persisting in the Vitiaz detached slab probably must propagate beyond the boundaries of the metastable region in order to account for the observed seismic activity (Van Ark et al., 1998).

7. Thermal effects

To the extent that disequilibrium conditions allow metastable persistence of lower pressure phases, the thermal evolution of slab material may also be affected. For example, latent heat release by exothermic phase transitions in subducting slab material is significantly enhanced (Fig. 12) under disequilibrium relative to equilibrium conditions (Daessler and Yuen, 1993, 1996; Rubie and Ross, 1994; Green and Houston, 1995; Green and Zhou, 1996; Kirby et al., 1996; Daessler et al., 1996; Devaux et al., 1997; Bina, 1998b). Hence, delayed transformation of metastable material may lead to local superheating, potentially accompanied by shear instability and seismicity (Griggs and Handin, 1960; Ogawa, 1987; Hobbs and Ord, 1988; Karato, 1997; Regenauer-Lieb and Yuen, 1998; Bina, 1998b; Regenauer-Lieb et al., 1999; Raterron et al., 1999). Furthermore, while recent attempts to incorporate spatially varying (temperature-dependent) thermal conductivity into slab models predict somewhat warmer slabs (Hauck et al., 1999), models employing temperature-dependent thermal diffusivity do predict enhanced development of such shear instability within the stability fields of the high-pressure olivine polymorphs in cold subducting slabs (Branlund et al., 2000).

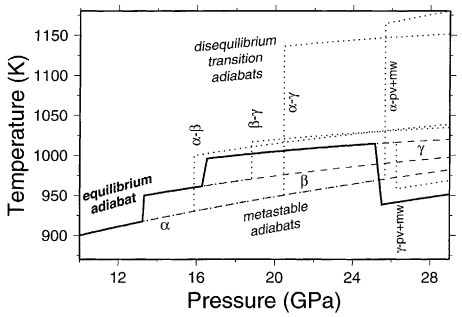

Fig. 12. For exothermic phase transitions in subducting slab material, latent heat release under disequilibrium conditions (dotted) from metastably persisting phases (dashed) is significantly enhanced relative to equilibrium conditions (solid). Adiabats calculated for transformations in forsterite (modified from Bina, 1998b).

In addition to perturbing subsolidus phase transformations, the low temperatures in subducting slabs may also affect dehydration reactions. Progressive dehydration of subducting slab material generally liberates water as a fluid phase which plays important roles in island-arc magmatism and intermediate-depth seismicity. In the coldest subduction zones, however, the stable phase of water may be solid ice VII rather than a fluid. For example, finite difference (Minear and Toksöz, 1970) thermal models for slabs possessing a variety of thermal parameters (Kirby et al., 1996) suggest that the Tonga slab may remain sufficiently cold for dehydration to occur within the ice VII stability field. The resulting shifts in reaction boundaries and relative buoyancies would significantly affect H_2O transport in subduction zones, altering patterns of seismicity, magmatism, and geochemistry (Bina and Navrotsky, 2000). The lower mobility of water in solid form could allow transport of greater amounts of H_2O below the nominal depths of dehydration reactions. Even in the absence of ice, however, H_2O can be transported by slabs deep within the mantle through the vehicle of dense hydrous magnesium silicate phases, stabilized by the low temperatures in slabs (Wood et al., 1996; Bose and Navrotsky, 1998).

8. Conclusions

Perturbation of mantle phase relations by the cold thermal environment of a subducting slab yields anomalies in the spatial distribution not only of seismic velocities but also of density, and these density anomalies give rise to significant buoyancy forces. These buoyancy forces manifest themselves in a number of ways. They contribute to the stress field within the slab in a manner reflected in observed patterns of the distribution of both moment release and focal mechanisms of deep seismicity. They may affect

subduction rates, both by introducing time-dependent velocity changes as slabs encounter equilibrium phase boundaries and by limiting the subduction rates of cold slabs in which buoyant metastable mineral phases persist under disequilibrium conditions. These buoyancy forces also may induce changes in slab morphology, allowing the temporary stagnation of deflected or detached slabs. While equilibrium buoyancy forces should remain important even in recumbent or detached slabs, any metastably persisting material may be subject to rapid thermal erosion in such environments.

While latent heats of phase transitions in subducting slabs under equilibrium conditions are simply manifested by refraction of adiabats along phase boundaries, latent heat release from exothermic phase transformations under disequilibrium conditions results in isobaric superheating above the equilibrium adiabat. Indeed, even nominally endothermic transitions can yield heating under sufficient metastable overpressure (Bina, 1998b). Thus, eventual transformation of any pods of metastable material should lead to local superheating which, if coupled to a strongly temperature-dependent viscosity, may lead to thermal runaway by strain localization and viscous shear heating. Such adiabatic instability may allow seismogenesis to nucleate in metastable material yet propagate well beyond its confines. The occurrence of such adiabatic shear instability in lithosphere near the surface is supported by field observations of pseudotachylite (Obata and Karato, 1995), and it is also manifest in numerical models of lithospheric necking (Regenauer-Lieb and Yuen, 1998, 2000). The role of shear instabilities in subducting lithosphere, on the other hand, remains speculative (Ogawa, 1987; Hobbs and Ord, 1988; Bina, 1998b), but recent numerical models of such processes do suggest its plausibility at the low temperatures of slab interiors (Regenauer-Lieb and Yuen, 1998; Branlund et al., 2000), and recent experimental results do suggest a role for plastic deformation in stress instabilities observed in olivine at high-pressures (Raterron et al., 1999).

Acknowledgements

We thank Th. Becker, O. Čadek, P.-F. Chen, W.-P. Chen, H. Green, A. Hook, E. Okal, S. Karato, S. Kirby, K. Kumayama, L. Leffler, C. Parks, D. Rubie, R. Russo, H. Schmeling, N. Sleep, V. Steinbach, H. Weertman, M. Woods, D. Yuen, and S. Yoshioka for stimulating discussions of various portions this work. For helpful discussions of software packages, we are grateful to J. Gobat (FElt), R. Foerch (Zebulon), and P. Wessel (GMT). All figures were produced using the GMT graphics package (Wessel and Smith, 1995). R. van der Hilst provided thoughtful comments on the manuscript. CRB acknowledges the support of the US National Science Foundation (EAR-9158594, EAR-9316396, INT-9603234, EAR-9706152), Princeton University (CHiPR), and the University of Tokyo (ERI). We thank the Alfred–Wegener–Stiftung for support of the 1999 Conference on Processes and Consequences of Deep Subduction in Verbania-Pallanza, Italy.

References

Akaogi, M., Ito, E., 1993. Refinement of enthalpy measurement of $MgSiO_3$ perovskite and negative pressure–temperature slopes for perovskite-forming reactions. Geophys. Res. Lett. 20, 1839–1842.

Akaogi, M., Ito, E., Navrotsky, A., 1989. Olivine modified spinel–spinel transitions in the system Mg_2SiO_4–Fe_2SiO_4: calorimetric measurements, thermochemical calculation, and geophysical application. J. Geophys. Res. 94, 15671–15685.

Akaogi, M., Navrotsky, A., Yagi, T., Akimoto, S., 1987. Pyroxene-garnet transformation: thermochemistry and elasticity of garnet solid solutions, and application to a pyrolite mantle. In: Manghnani, M.H., Syono, Y. (Eds.), High-Pressure Research in Mineral Physics. American Geophysical Union, Washington, DC, pp. 251–260.

Bassett, W.A., 1979. The diamond cell and the nature of the Earth's mantle. Ann. Rev. Earth Planet. Sci. 7, 357–384.

Batchelor, G.K., 1967. An Introduction to Fluid Dynamics. Cambridge University, New York.

Becker, Th.W., Faccenna, C., O'Connell, R.J., Giardini, D., 1999. The development of slabs in the upper mantle: insight from numerical and laboratory experiments. J. Geophys. Res. 104, 15207–15226.

Bevis, M., Taylor, F.W., Schutz, B.E., Recy, J., Isacks, B.L., Helu, S., Singh, R., Kendrick, E., Stowell, J., Taylor, B., Calmant, S., 1995. Geodetic observations of very rapid convergence and back-arc extension at the Tonga arc. Nature 374, 249–251.

Bina, C.R., 1996. Phase transition buoyancy contributions to stresses in subducting lithosphere. Geophys. Res. Lett. 23, 3563–3566.

Bina, C.R., 1997. Patterns of deep seismicity reflect buoyancy stresses due to phase transitions. Geophys. Res. Lett. 24, 3301–3304.

Bina, C.R., 1998a. Free energy minimization by simulated annealing with applications to lithospheric slabs and mantle plumes. Pure Appl. Geophys. 151, 605–618.

Bina, C.R., 1998b. A note on latent heat release from disequilibrium phase transformations and deep seismogenesis. Earth Planets Space 50, 1029–1034.

Bina, C.R., Helffrich, G., 1994. Phase transition Clapeyron slopes and transition zone seismic discontinuity topography. J. Geophys. Res. 99, 15853–15860.

Bina, C.R., Kirby, S.H., 1999. Model estimates of the petrological buoyancy cost of descent into the transition zone and lower mantle of slabs containing metastable olivine: results for the Tonga subduction zone. Eos Trans. Am. Geophys. Union 80, Spring Suppl., S31B–09.

Bina, C.R., Liu, M., 1995. A note on the sensitivity of mantle convection models to composition-dependent phase relations. Geophys. Res. Lett. 22, 2565–2568.

Bina, C.R., Navrotsky, A., 2000. Possible presence of high-pressure ice in cold subducting slabs. Nature 408, 844–847.

Bina, C.R., Wood, B.J., 1984. The eclogite to garnetite transition: experimental and thermodynamic constraints. Geophys. Res. Lett. 11, 955–958.

Bose, K., Navrotsky, A. 1998. Thermochemistry and phase equilibria of hydrous phases in the system $MgO–SiO_2–H_2O$: implications for volatile transport to the mantle. J. Geophys. Res. 103, 9713-9719.

Branlund, J.M., Kameyama, M.C., Yuen, D.A., Kaneda, Y., 2000. Effects of temperature-dependent thermal diffusivity on shear instability in a viscoelastic zone: implications for faster ductile faulting and earthquakes in the spinel stability field. Earth Planet. Sci. Lett. 182, 171–185.

Brudzinski, M.R., Chen, W.-P., 2000. Variations of P-wave speeds and outboard earthquakes: evidence for a petrologic anomaly in the mantle transition zone. J. Geophys. Res. 105, 21661–21682.

Brudzinski, M.R., Chen, W.-P., Nowack, R.L., Huang, B.-S., 1997. Variations of P-wave speeds in the mantle transition zone beneath the Northern Philippine Sea. J. Geophys. Res. 102, 11815–11827.

Christensen, U.R., Yuen, D.A., 1984. The interaction of a subducting lithospheric slab with a chemical or phase boundary. J. Geophys. Res. 89, 4389–4402.

Christensen, U.R., Yuen, D.A., 1985. Layered convection induced by phase transitions. J. Geophys. Res. 90, 10291–10300.

Collier, J.D., Helffrich, G.R., 1997. Topography of the 410 and 660 km seismic discontinuities in the Izu–Bonin subduction zone. Geophys. Res. Lett. 24, 1535–1538.

Collier, J., Helffrich, G., 2000. Seismic discontinuities and subduction zones. In: Processes and Consequences of Deep Subduction, Rubie, D., van der Hilst, R.D. (Eds.), Phys. Earth Planet. Inter., this volume.

Daessler, R., Yuen, D.A., 1993. The effects of phase transition kinetics on subducting slabs. Geophys. Res. Lett. 20, 2603–2606.

Daessler, R., Yuen, D.A., 1996. The metastable olivine wedge in fast subducting slabs: constraints from thermo-kinetic coupling. Earth Planet. Sci. Lett. 137, 109–118.

Daessler, R., Yuen, D.A., Karato, S., Riedel, M.R., 1996. Two-dimensional thermo-kinetic model for the olivine-spinel phase transition in subducting slabs. Phys. Earth Planet. Int. 94, 217–239.

Deal, M.M, Nolet, G., 1999. Slab temperature and thickness from seismic tomography. Part 1. Method and application to Tonga. J. Geophys. Res. 104, 28789–28802.

Devaux, J.P., Schubert, G., Anderson, C., 1997. Formation of a metastable olivine wedge in a descending slab. J. Geophys. Res. 102, 24627–24637.

Devaux, J.P., Fleitout, L., Schubert, G., Anderson, C., 1999. Stresses in a subducting slab in the presence of a metastable olivine wedge. J. Geophys. Res. 105, 13365–13374.

Dziewonski, A.M., Hales, A.L., Lapwood, E.R., 1975. Parametrically simple Earth models consistent with geophysical data. Phys. Earth Planet. Int. 10, 12–48.

Elsasser, W.M., 1969. Convection and stress propagation in the upper mantle. In: Runcorn, S.K. (Ed.), The Application of Modern Physics to the Earth and Planetary Interiors. Wiley, New York, pp. 223–246.

Fei, Y., Mao, H.-K., Mysen, B.O., 1991. Experimental determination of element partitioning and calculation of phase relations in the $MgO–FeO–SiO_2$ system at high-pressure and high temperature. J. Geophys. Res. 96, 2157–2170.

Forsyth, D.W., Uyeda, S., 1975. On the relative importance of the driving forces of plate motion. Geophys. J.R. Astron. Soc. 43, 163–200.

Frohlich, C., 1989. The nature of deep-focus earthquakes. Ann. Rev. Earth Planet. Sci. 17, 227–254.

Fukao, Y., Widiyantoro, S., Obayashi, M., 2001. Stagnant slabs in the upper and lower mantle transition region. Rev. Geophys. 39, 291–323.

Gobat, J.I., Atkinson, D.C., 1995. The FElt System: User's Guide and Reference Manual, Computer Science Technical Report. University of California, San Diego, pp. CS94–376.

Gorbatov, A., Kostoglodov, V., Burov, E., 1996. Maximum seismic depth versus thermal parameters of subducted slab: application to deep earthquakes in Chile and Bolivia. Geofis. Int. 35, 41–50.

Gordon, R.G., 1991. Plate tectonic speed limits. Nature 349, 16–17.

Gordon, R.G., Jurdy, D.M., 1986. Cenozoic global plate motions. J. Geophys. Res. 91, 12389–12406.

Goto, K., Suzuki, Z., Hamaguchi, H., 1987. Stress distribution due to olivine-spinel phase transition in descending plate and deep focus earthquakes. J. Geophys. Res. 92, 13811–13820.

Green, H.W. II, Burnley, P., 1989. A new self-organizing mechanism for deep-focus earthquakes. Nature 338, 753.

Green, H.W. II, Houston, H., 1995. The mechanics of deep earthquakes. Ann. Rev. Earth Planet. Sci. 23, 169–213.

Green, H.W. II, Zhou, Y., 1996. Transformation-induced faulting requires an exothermic reaction and explains the cessation of earthquakes at the base of the mantle transition zone. Tectonophys. 256, 39–56.

Greene, H.G., Collot, J.Y., Fisher, M.A., Crawford, A.J., 1994. Neogene tectonic evolution of the New Hebrides island-arc: a review incorporating ODP drilling results. Proc. ODP Sci. Results 134, 19–46.

Griggs, D., 1972. The sinking lithosphere and the focal mechanism of deep earthquakes. In: Robertson, E.C. (Ed.), The Nature of the Solid Earth. McGraw-Hill, New York, pp. 361–384.

Griggs, D., Handin, J., 1960. Observations on fracture and a hypothesis of earthquakes. In: Griggs, D., Handin, J. (Eds.), Rock Deformation, Memoir 79. Geological Society America, New York, pp. 347–364.

Hamburger, M.W., Isacks, B.L., 1987. Deep earthquakes in the southwest Pacific: a tectonic interpretation. J. Geophys. Res. 92, 13841–13854.

Hauck, S.A., II, , Phillips, R.J., Hofmeister, A.M., 1999. Variable conductivity: effects on the thermal structure of subducting slabs. Geophys. Res. Lett. 26, 3257–3260.

Helffrich, G., 1998. Comment on 'seismological evidence for the existence of anisotropic zone in the metastable wedge inside the subducting Izu-Bonin slab' by T. Iidaka and K. Obara. Geophys. Res. Lett. 25, 3243–3244.

Helffrich, G., 2000. Topography of the transition zone seismic discontinuities. Rev. Geophys. 38, 141–158.

Helffrich, G., Bina, C.R., 1994. Frequency dependence of the visibility and depths of mantle seismic discontinuities. Geophys. Res. Lett. 21, 2613–2616.

Helffrich, G., Brodholt, J., 1991. Relationship of deep seismicity to the thermal structure of subducted lithosphere. Nature 353, 252–255.

Helffrich, G., Stein, S., Wood, B.J., 1989. Subduction zone thermal structure and mineralogy and their relationship to seismic wave reflections and conversions at the slab/mantle interface. J. Geophys. Res. 94, 753–763.

Hobbs, B.E., Ord, A., 1988. Plastic instabilities: implications for the origin of intermediate and deep focus earthquakes. J. Geophys. Res. 93, 10521–10540.

Hogrefe, A., Rubie, D.C., Sharp, T.G., Seifert, F., 1994. Metastability of enstatite in deep subducting lithosphere. Nature 372, 351–353.

Houston, H., Williams, Q., 1991. Fast rise times and the physical mechanism of deep earthquakes. Nature 352, 520–522.

Iidaka, T., Obara, K., 1997. Seismological evidence for the existence of anisotropic zone in the metastable wedge inside the subducting Izu–Bonin slab. Geophys. Res. Lett. 24, 3305–3308.

Isacks, B., Molnar, P., 1971. Distribution of stresses in the descending lithosphere from a global survey of focal-mechanism solutions of mantle earthquakes. Rev. Geophys. Space Phys. 9, 103–174.

Ito, E., Akaogi, M., Topor, L., Navrotsky, A., 1990. Negative pressure–temperature slopes for reactions forming $MgSiO_3$ perovskite from calorimetry. Science 249, 1275–1278.

Ito, E., Sato, H., 1992. Effect of phase transformations on the dynamics of the descending slab. In: Syono, Y., Manghnani, M.H. (Eds.), High-Pressure Research: Application to Earth and Planetary Sciences. American Geophysical Union, Washington, DC, pp. 257–262.

Ito, E., Takahashi, E., 1989. Post-spinel transformations in the system Mg_2SiO_4–Fe_2SiO_4 and some geophysical implications. J. Geophys. Res. 94, 10637–10646.

Karato, S.-I., 1997. Phase transformations and rheological properties of mantle minerals. In: Crossley, D.J. (Ed.), Earth's Deep Interior: The Doornbos Memorial Volume. Gordon and Breach, Amsterdam, pp. 223–272.

Katsura, T., Ito, E., 1989. The system Mg_2SiO_4–Fe_2SiO_4 at high-pressures and temperatures: precise determination of stabilities of olivine, modified spinel, and spinel. J. Geophys. Res. 94, 15663–15670.

Kerschhofer, L., Sharp, T.G., Rubie, D.C., 1996. Intracrystalline transformation of olivine to wadsleyite and ringwoodite under subduction zone conditions. Science 274, 79–81.

Kirby, S.H., Durham, W.B., Stern, L., 1991. Mantle phase changes and deep-earthquake faulting in subducting slabs. Science 252, 216–225.

Kirby, S.H., Stein, S., Okal, E.A., Rubie, D.C., 1996. Metastable mantle phase transformations and deep earthquakes in subducting oceanic lithosphere. Rev. Geophys. 34, 261–306.

Koper, K.D., Wiens, D.A., 2000. The waveguide effect of metastable olivine in slabs. Geophys. Res. Lett. 27, 581–584.

Koper, K.D., Wiens, D.A., Dorman, L.M., Hildebrand, J.A., Webb, S.C., 1998. Modeling the Tonga slab: can travel time data resolve a metastable olivine wedge? J. Geophys. Res. 103, 30079–30100.

Lay, T., 1994. The fate of subducting slabs. Ann. Rev. Earth Planet. Sci. 22, 33–61.

Lithgow-Bertelloni, C., Richards, M.A., 1998. The dynamics of Cenozoic and Mesozoic plate interiors. Rev. Geophys. 36, 27–78.

Liu, M., Kerschhofer, L., Mosenfelder, J.L., Rubie, D.C, 1998. The effect of strain energy on growth rates during the olivine-spinel transformation and implications for olivine metastability in subducting slabs. J. Geophys. Res. 103, 23897–23909.

Lundgren, P., Giardini, D., 1992. Seismicity, shear failure and modes of deformation in deep subduction zones. Phys. Earth Planet. Int. 74, 63–74.

Lundgren, P.R., Giardini, D., 1994. Isolated deep earthquakes and the fate of subduction in the mantle. J. Geophys. Res. 99, 15833–15842.

Marton, F.C., Bina, C.R., Stein, S., Rubie, D.C., 1999a. Effects of slab mineralogy on subduction rates. Geophys. Res. Lett. 26, 119–122.

Marton, F.C., Bina, C.R., Stein, S., Rubie, D.C., 1999b. Mineralogy and the regulation of subduction rates. Eos Trans. Am. Geophys. Union 80, Fall Suppl., T11G–08.

McKenzie, D.P., 1969. Speculations on the consequences and causes of plate motions. Geophys. J.R. Astrol. Soc. 18, 1–32.

Minear, J., Toksöz, M.N., 1970. Thermal regime of a downgoing slab and new global tectonics. J. Geophys. Res. 75, 1379–1419.

Mitrovica, J.X., Peltier, W.R., 1993. The inference of mantle viscosity from an inversion of the Fennoscandian relaxation spectrum. Geophys. J. Int. 114, 45–62.

Molnar, P., Freedman, D., Shih, J.S.F., 1979. Lengths of intermediate and deep seismic zones and temperatures in downgoing slabs of lithosphere. Geophys. J. Int. 6, 41–54.

NEIC, 1994. Catalogue of Preliminary Determinations of Epicenters (PDE), 1964–1994. National Earthquake Information Center, US Geological Survey, Denver.

Navrotsky, A., 1980. Lower mantle phase transitions may generally have negative pressure–temperature slopes. Geophys. Res. Lett. 7, 709–711.

Northwest Numerics, 1998. Zebulon Handbook, Version 7.2/8.0. Northwest Numerics and Modeling, Seattle.

Obata, M., Karato, S., 1995. Ultramafic pseudotachylite from the Balmuccia Peridotite, Ivrea-Verbano Zone, northern Italy. Tectonophysics 242, 313–328.

Ogawa, M., 1987. Shear instability in a viscoelastic material as the cause of deep focus earthquakes. J. Geophys. Res. 92, 13801–13810.

Okal, E.A., Bina, C.R., 1998. On the cessation of seismicity at the base of the transition zone. J. Seism. 2, 65–86. Erratum, J. Seism., 2, 377–381.

Okal, E.A., Kirby, S.H., 1998. Deep earthquakes beneath the Fiji Basin, SW Pacific: Earth's most intense deep seismicity in stagnant slabs. Phys. Earth Planet. Int. 109, 25–63.

Raterron, P., Wu, Y., Weidner, D.J., 1999. Olivine plastic instability as an alternative process for deep focus earthquakes? TEM investigation of high-pressure olivine samples exhibiting stress instabilities above 400°C. Eos Trans. Am. Geophys. Union 80, Fall Suppl., T22E–06.

Rees, B.A., Okal, E.A., 1987. The depth of the deepest historical earthquakes. Pure Appl. Geophys. 125, 699–715.

Regenauer-Lieb, K., Petit, J.P., Yuen, D.A., 1999. Adiabatic shear bands in the lithosphere: numerical and experimental approaches. Electron. Geosci. 4, 2.

Regenauer-Lieb, K., Yuen, D.A., 1998. Rapid conversion of elastic energy into plastic shear heating during incipient necking of the lithosphere. Geophys. Res. Lett. 25, 2737–2740.

Regenauer-Lieb, K., Yuen, D.A., 2000. Quasi-adiabatic instabilities associated with necking processes of an elasto–viscoplastic lithosphere. Phys. Earth Planet. Int. 118, 89–102.

Riedel, M.R., Karato, S., 1997. Grain-size evolution in subducted oceanic lithosphere associated with the olivine-spinel transformation and its effect on rheology. Earth Planet. Sci. Lett. 148, 27–43.

Richter, F.M., 1973. Finite amplitude convection through a phase boundary. Geophys. J.R. Astron. Soc. 35, 265–287.

Ringwood, A.E., 1982. Phase transformations and differentiation in subducted lithosphere: implications for mantle dynamics, basalt petrogenesis, and crustal evolution. J. Geol. 90, 611–643.

Roth, E.G., Wiens, D.A., 1999. Depression of the 660 km discontinuity beneath the Tonga slab determined from near-vertical ScS reverberations. Geophys. Res. Lett. 26, 1223–1226.

Rubie, D.C., 1993. Mechanisms and kinetics of solid state reconstructive phase transformations in the Earth's mantle. In: Luth, R.W. (Ed.), Short Course Handbook on Experiments at High-Pressure and Applications to the Earth's Mantle, Vol. 21. Mineral. Association Canada, Edmonton, pp. 247–303.

Rubie, D.C., Ross, C.R. II, 1994. Kinetics of the olivine-spinel transformation in subducting lithosphere: experimental constraints and implications for deep slab processes. Phys. Earth Planet. Int. 86, 223–241.

Schmeling, H., Monz, R., Rubie, D.C., 1999. The influence of olivine metastability on the dynamics of subduction. Earth Planet. Sci. Lett. 165, 55–66.

Schubert, G., Turcotte, D.L., Oxburgh, E.R., 1970. Phase change instability in the mantle. Science 169, 1075–1077.

Schubert, G., Yuen, D.A., Turcotte, D.L., 1975. Role of phase transitions in a dynamic mantle. Geophys. J.R. Astrol. Soc. 42, 705–735.

Segerlind, L.J., 1984. Applied Finite Element Analysis. Wiley, New York.

Stein, C.A., Stein, S., 1992. A model for the global variation in oceanic depth and heat flow with lithospheric age. Nature 359, 123–129.

Stixrude, L., 1997. Structure and sharpness of phase transitions and mantle discontinuities. J. Geophys. Res. 102, 14835–14852.

Sung, C.-M., Burns, R.G., 1976a. Kinetics of the high-pressure phase transformations: implications to the evolution of the olivine-spinel phase transition in the downgoing lithosphere and its consequences on the dynamics of the mantle. Tectonophysics 31, 1–32.

Sung, C.-M., Burns, R.G., 1976b. Kinetics of the olivine-spinel transition: implications to deep-focus earthquake genesis. Earth Planet. Sci. Lett. 32, 165–170.

Tetzlaff, M., Schmeling, H., 2000. The influence of olivine metastability on deep subduction of oceanic lithosphere. Phys. Earth Planet. Int. 120, 29–38.

Toksoz, M.N., Sleep, N.H., Smith, A.T., 1973. Evolution of the downgoing lithosphere and the mechanisms of deep focus earthquakes. Geophys. J.R. Astrol. Soc. 35, 285–310.

Turcotte, D.L., Schubert, G., 1971. Structure of the olivine-spinel phase boundary in the descending lithosphere. J. Geophys. Res. 76, 7980–7987.

Turcotte, D.L., Schubert, G., 1972. Correction. J. Geophys. Res. 77, 2146.

Vacher, P., Moquet, A., Sotin, C., 1998. Computation of seismic profiles from mineral physics: the importance of the non-olivine components for explaining the 660 km discontinuity. Phys. Earth Planet. Int. 106, 275–298.

Vacher, P., Spakman, W., Wortel, M.J.R., 1999. Numerical test on the seismic visibility of metastable minerals in subduction zones. Earth Planet. Sci. Lett. 170, 335–349.

Van Ark, E.M., Marton, F.C., Bina, C.R., Stein, S.A., Rubie, D., 1998. Survival of metastable olivine in detached slabs: difficult but not impossible. Eos Trans. Am. Geophys. Union 79, Spring Suppl., S164.

Vassiliou, M.S., Hager, B.H., 1988. Subduction zone earthquakes and stress in slabs. Pure Appl. Geophys. 128, 547–624.

Vassiliou, M.S., Hager, B.H., Raefsky, A., 1984. The distribution of earthquakes with depth and stress in in subducting slabs. J. Geodynam. 1, 11–28.

Wang, Y., Martinez, I., Guyot, F., Liebermann, R.C., 1997. The breakdown of olivine to perovskite and magnesiowüstite. Science 275, 510–513.

Wessel, P., Smith, W.H.F., 1995. New version of the generic mapping tools released. Eos Trans. Am. Geophys. Union 76, 329.

Wood, B.J., Pawley, A., Frost, D.R., 1996. Water and carbon in the Earth's mantle. Phil. Trans. R. Soc. Lond. A 354, 1495–1511.

Wood, B.J., Rubie, D.C., 1996. The effect of alumina on phase transformations at the 660-km discontinuity from Fe–Mg partitioning experiments. Science 273, 1522–1524.

Yoshioka, S., Daessler, R., Yuen, D.A., 1997. Stress fields associated with metastable phase transitions in descending slabs and deep-focus earthquakes. Phys. Earth Planet. Int. 104, 345–361.

van der Hilst, R.D., 1995. Complex morphology of subducted lithosphere in the mantle beneath the Tonga trench. Nature 374, 154–157.

Zhao, D., Xu, Y., Wiens, D.A., Dorman, L., Hildebrand, J., Webb, S., 1997. Depth extent of the Lau back-arc spreading center and its relationship to subduction processes. Science 278, 254–257.